

ULTURB

Scientific Description

Background

To date, clear air turbulence (CAT) forecast techniques have been an amalgamation of mostly empirical rules and equations, most of which are based on perceived connections between observed atmospheric patterns and aircraft turbulence reports. McCann (2001) demonstrated that these techniques look at the environmental setup for CAT as measured directly or indirectly by the Richardson number

$$Ri \equiv \frac{1}{\Theta} \frac{d\Theta}{dz} \frac{1}{\left(\frac{d\mathbf{V}}{dz}\right)^2}$$

where Θ is the potential temperature and \mathbf{V} is the wind velocity. The numerator is the layer's stability, and the denominator is the layer's wind shear.

Layers above the atmospheric boundary layer are rarely favorable for turbulence because it is necessary for $Ri < 0.25$ for turbulence to form. Assumed in these techniques is some undefined process that locally alters the environment so the atmosphere can become turbulent. The lower the environmental Ri , the higher probability of turbulence. Unfortunately, these techniques overforecast CAT because often low Ri environments are smooth. The situation is analogous to thunderstorm forecasting only considering conditional instability. Indeed, the thunderstorm probability increases with a lower Lifted Index, but successful thunderstorm forecasts include consideration of triggers. Similarly, CAT forecasting techniques that include a trigger analysis should reduce the uncertainty of environment-only techniques.

Gravity waves, which are ubiquitous in the atmosphere, alter both the environmental wind shear and the stability as they move through. McCann showed that, under the influence of a gravity wave, the local Richardson number (Ri_L):

$$Ri_L = Ri_E \frac{1 + \hat{a} \cos \varphi}{\left(1 + Ri_E^{1/2} \hat{a} \sin \varphi\right)^2}$$

where Ri_E is the environmental Richardson number, φ is the gravity wave phase angle, and \hat{a} is the wave amplitude non-dimensionalized by multiplying the actual wave amplitude by the stability and dividing by the Doppler-adjusted wind speed, $|\mathbf{V}-\mathbf{c}|$, where \mathbf{c} is the wave phase velocity. There are sufficient observations/numerical model forecasts of the wind and temperature to compute environmental stability, wind shear, and Ri_E . The gravity wave amplitude and phase velocity are unknowns that make computing Ri_L difficult. Obviously, better knowledge of gravity wave characteristics will allow forecasters to apply the theory with confidence.

However, assuming that \hat{a} can be computed in some way, the formula shows the local increases or decreases in stability and wind shear within the gravity wave oscillation depending on the gravity wave phase angle, φ . Turbulence forecasters are only interested in the modifications that will produce Ri_L less than 0.25. When $\varphi = \pi$ and $\hat{a} > 1$, $Ri_L < 0.0$, a condition for wave breaking. When $\varphi = \pi/2$, the local wind shear is maximized, so when $Ri_E(2-\hat{a}) < 1$, then $Ri_L < 0.25$. For $\hat{a} > 2$, Ri_L is always less than 0.25. Figure 1 depicts the graph of this curve. As $\hat{a} \rightarrow 2$, the upper limit on Ri_E for turbulence approaches infinity. Below the curve are Ri_E and \hat{a} combinations that are turbulent.

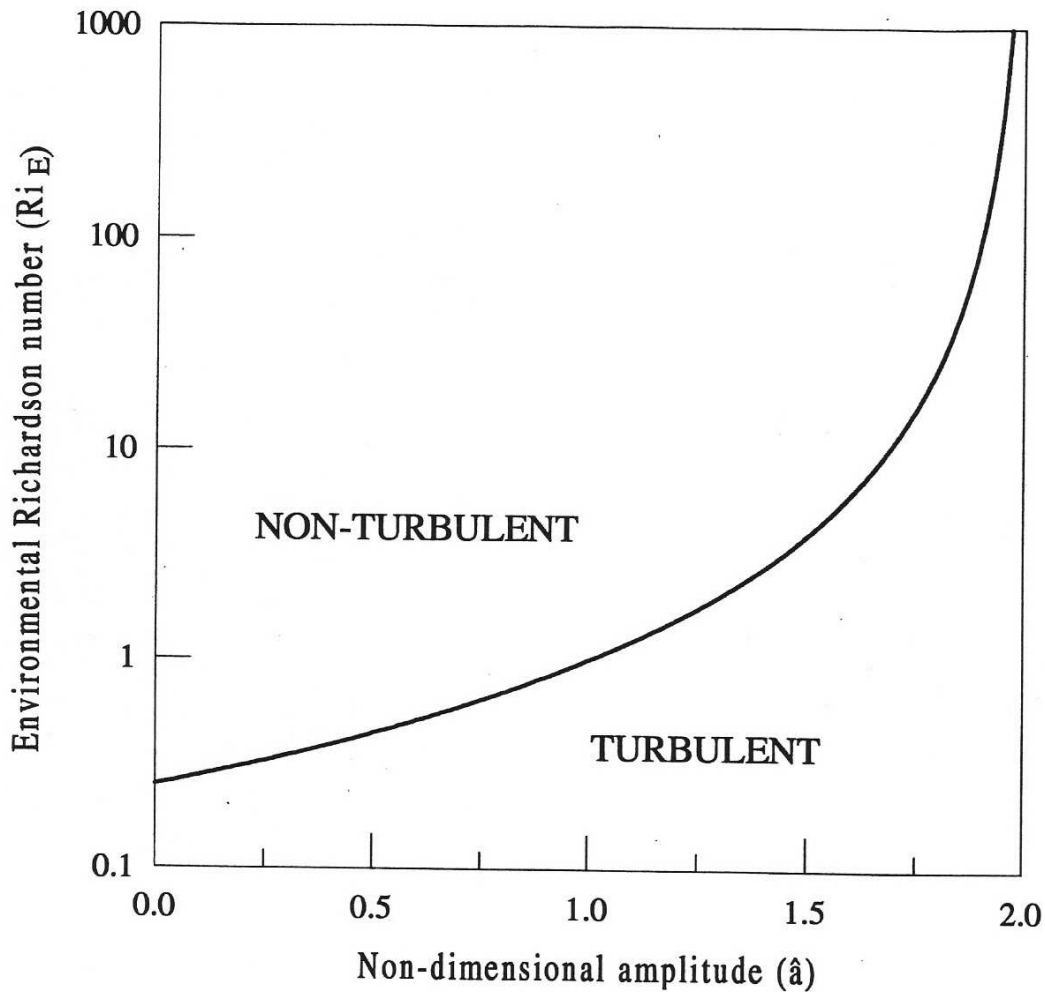


Figure 1. Curve of the bounding value of the environmental Richardson number as a function of the non-dimensional amplitude (\hat{a}). When \hat{a} falls in the TURBULENT region, a gravity wave will locally increase the wind shear sufficiently to reduce the local Richardson number to < 0.25 .

This theory quantifies current environmental-only CAT forecast techniques. The lower the environmental Richardson number, the higher the probability that a gravity wave with sufficient non-dimensional amplitude will reduce the local Richardson number to less than 0.25.

If gravity waves trigger CAT in this manner, then improving CAT forecasting techniques requires future knowledge of the gravity waves that cause CAT. There are many sources of gravity waves, and any gravity wave may be a potential turbulence producer. Topographically

forced gravity waves are often turbulent (Lilly 1978, Bacmeister et al. 1994, McCann 2006). In fact, Bacmeister et al. and McCann use a technique derived by Macfarlane (1987) which computes a local Richardson number from the equation above. The non-dimensional wave amplitude is estimated from the mountain height and environmental stability and wind speed profile above the mountain.

When one horizontal force on an air parcel changes radically, the parcel may begin to oscillate and excite gravity waves. The vertical acceleration of a parcel is proportional to the local change in divergence as can be shown by taking the time derivative of continuity equation. Sharman et al. 2006 and Knox et al. 2006 have implemented marginally successful turbulence diagnostics based on the divergence tendency, however, these have been only statistical diagnostics. Unknown still is a relationship between divergence tendency and gravity wave amplitude that can be plugged into the local Richardson number equation above.

Vortical flow can also emit gravity waves spontaneously (Lighthill 1952 and Ford 1994). Williams et al. (2005) explored gravity wave development in rotating annulus experiments. Of the five dynamical indicators tested, the most accurate was that of Lighthill-Ford spontaneous imbalance. Knox et al (2007) derived an applications-friendly version of the Lighthill-Ford equations and applied it to the McCann (2001) turbulence forecasting method.

Lighthill-Ford Spontaneous Imbalance

The Lighthill-Ford equation describes how gravity waves can be emitted in vortical flow. The equation arises by combining the divergence and vorticity equations with the conservation of mass equation and its second derivative. Nonzero values are a source for gravity waves. The expression for Lighthill-Ford radiation are not convenient for interpretation and application. Knox et al. (2007) expanded each of the three radiation terms.

Radiation term 1 (R_1) can be expressed as a function of the horizontal divergence D :

$$R_1 = 2 \left[\underbrace{\frac{\partial}{\partial t} D^2}_{\text{Term 1A}} + \underbrace{\frac{\partial}{\partial t} \mathbf{V} \cdot \nabla D}_{\text{Term 1B}} - \underbrace{\frac{\partial}{\partial t} J(u, v)}_{\text{Term 1C}} \right]$$

Where \mathbf{V} is the horizontal wind and $J(u, v)$ is the Jacobian of the u- and v-components of the wind. Term 1A is a source term due to the local change of divergence; Term 1B is a source of gravity waves via the local change of the horizontal advection of horizontal divergence. Term 1C is the time derivative of the familiar Jacobian term found in the divergence tendency equation.

Radiation term 2 (R_2) is a combination of the horizontal divergence and the vertical component of relative vorticity •:

$$R_2 = f \left[\underbrace{2D\zeta}_{\text{Term 2A}} + \underbrace{\mathbf{V} \cdot \nabla \zeta}_{\text{Term 2B}} + \underbrace{\left(v \frac{\partial D}{\partial x} - u \frac{\partial D}{\partial y} \right)}_{\text{Term 2C}} \right]$$

The product of divergence and relative vorticity is found in Term 2A. Term 2B is the horizontal advection of relative vorticity. Term 2C is proportional to the vertical component of the cross-product of the vector velocity with the horizontal gradient of divergence.

Radiation term 3 can also be re-expressed as:

$$R_3 = g \left[\underbrace{\frac{\partial h}{\partial t} \nabla^2 h}_{\text{Term 3A}} + \underbrace{(h - h_0) \left(\nabla^2 \frac{\partial h}{\partial t} \right)}_{\text{Term 3B}} + 2 \underbrace{\left(\frac{\partial h}{\partial x} \frac{\partial^2 h}{\partial t \partial x} + \frac{\partial h}{\partial y} \frac{\partial^2 h}{\partial t \partial y} \right)}_{\text{Term 3C}} \right]$$

A simple scale analysis of the radiation subterms for conditions representative of many clear-air turbulence outbreaks shows that term 2B dominates. It is an order of magnitude larger than the three next dominate subterms, terms 1C, 2A, and 2C. The remaining subterms, 1A, 1B, and 3, are an order of magnitude even smaller.

Therefore, large advection of relative vorticity should be a dominant source of spontaneous gravity wave generation. The Jacobian term, divergence-vorticity product, and cross-product of velocity with the gradient of divergence may also play non-negligible roles.

The ULTURB algorithm

With the hypothesis that gravity waves radiate in conditions described by Lighthill-Ford theory, it is further hypothesized that the absolute value of the total radiation may be used to estimate \hat{a} . There is a lack of consensus about the scaling properties of inertia-gravity wave amplitudes in theories and atmospheric observations, but in laboratory experiments (Williams et al. 2007, submitted to *J. Atmos. Sci.*), the inertia-gravity waves generated have an amplitude which scale with the square root of the Lighthill-Ford radiation:

$$\hat{a}^2 \propto R = \mathbf{f}\mathbf{u} \cdot \nabla \zeta + 2Df\zeta - \mathbf{f}\mathbf{k} \cdot \mathbf{u} \times \nabla D - 2 \frac{\partial}{\partial t} J(u, v)$$

Knox et al. (2007) empirically determined the proportionality by matching distributions of pilot reports in strong CAT outbreaks.

The instantaneous time derivative of the Jacobian (term 1C) is

$$\frac{\partial}{\partial t} J(u, v) = J\left(\frac{\partial u}{\partial t}, v\right) + J\left(u, \frac{\partial v}{\partial t}\right),$$

and the time derivatives are calculated from the equation of motion via

$$\begin{aligned}\frac{\partial u}{\partial t} &= -\frac{\partial \Phi}{\partial y} - fv - u \frac{\partial u}{\partial x} - v \frac{\partial u}{\partial y} \\ \frac{\partial v}{\partial t} &= \frac{\partial \Phi}{\partial x} - fu - u \frac{\partial v}{\partial x} - v \frac{\partial v}{\partial y},\end{aligned}$$

where Φ is the geopotential height.

Knowing \hat{a} , the maximum production of turbulent kinetic energy (TKE_{wshr}) from gravity wave enhanced wind shear is (McCann 2001):

$$TKE_{wshr} = K_m \left(\frac{\partial \mathbf{V}}{\partial z} \right)^2 (1 + \hat{a} \sqrt{Ri_E})^2 \quad \hat{a} > \left(2 - \frac{1}{Ri_E} \right)$$

where K_m is the momentum eddy diffusivity or eddy viscosity. The maximum turbulent kinetic energy from gravity wave enhanced buoyancy (TKE_{buoy}) is

$$TKE_{buoy} = K_h (\hat{a} - 1) N^2 \quad \hat{a} > 1$$

where K_h is the eddy thermal diffusivity and $N^2 = \frac{g}{\Theta} \frac{\partial \Theta}{\partial z}$, in which Θ the potential temperature.

The ratio, K_m / K_h , is a turbulent Prandtl number; the closer this ratio is to 0.25, the less intermittent the turbulence. The eddy viscosity is empirically determined so that the resulting TKE dissipation estimates the eddy dissipation rate of actual aircraft (Cornman et al. 1995). The eddy thermal diffusivity, $K_h = 4 K_m$.

At each model grid point and in each layer, ULTURB first computes the Lighthill-Ford radiation. ULTURB determines TKE production in two ways: 1) if the (\hat{a}, Ri) combination is below the curve in Fig. 1, then ULTURB computes the enhanced TKE_{wshr} , and 2) if $\hat{a} > 1$, then ULTURB computes the enhanced TKE_{buoy} . ULTURB limits the non-dimensional amplitude, $\hat{a} = 2.5$ to account for nonlinear limitations on wave amplification. The maximum of the two TKE productions is the final value at the grid point.

Operational interpretation

The following figures show a severe turbulence outbreak case on 9 March 2006. Using the 1-hour RUC2 forecast from 0000 UTC 10 March 2006, ULTURB calculated the TKE production using the Lighthill-Ford gravity wave forcing shown in Figure 2. Figure 3 depicts 200-225 hPa TKE dissipation overlaid with PIREPs of turbulence occurring between FL350 and FL410 (FL is hundreds of feet above mean sea level). By comparison, the 25-hPa layer (200-225 hPa) bulk Richardson number (Figure 2) indicates very broad regions of $Ri < 1$ across much of Illinois, southern Wisconsin, and parts of Michigan.

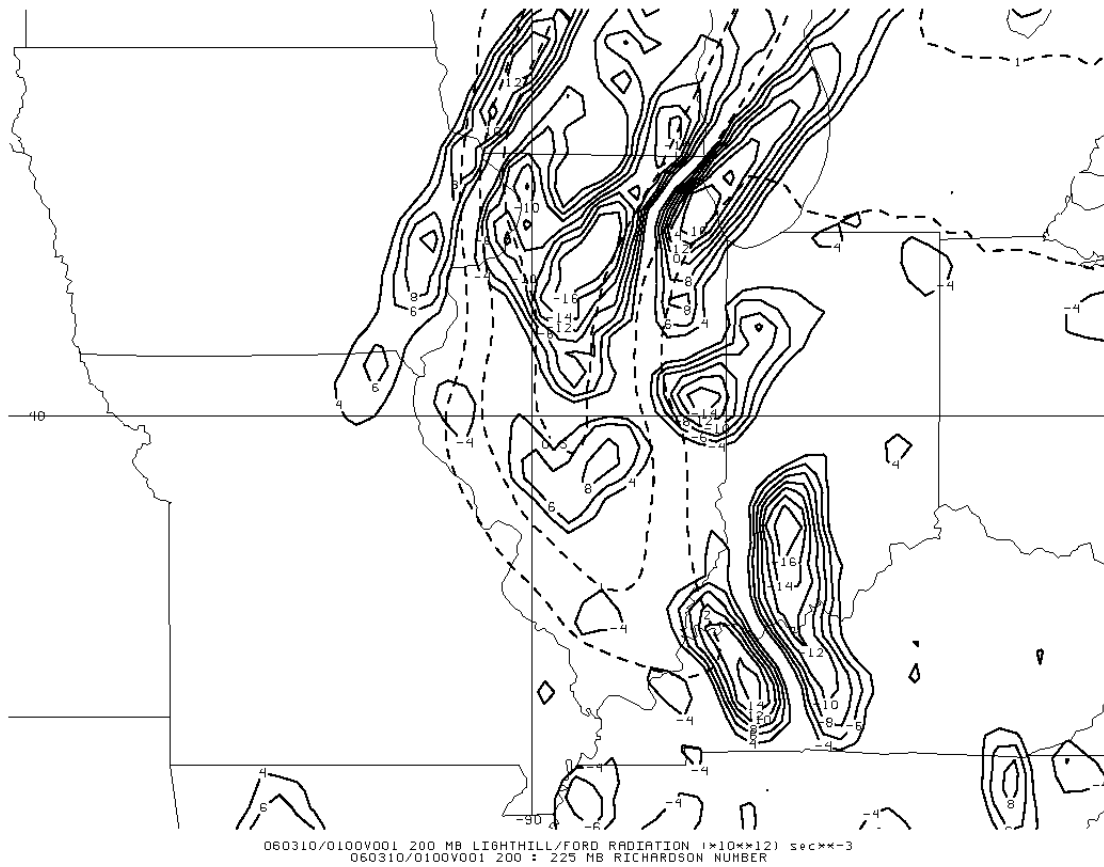


Figure 2. Lighthill-Ford radiation (solid lines) and 200-225 hPa Richardson number (dashed lines) using the 1-hour RUC2 forecast at 0000 UTC 10 March 2006.

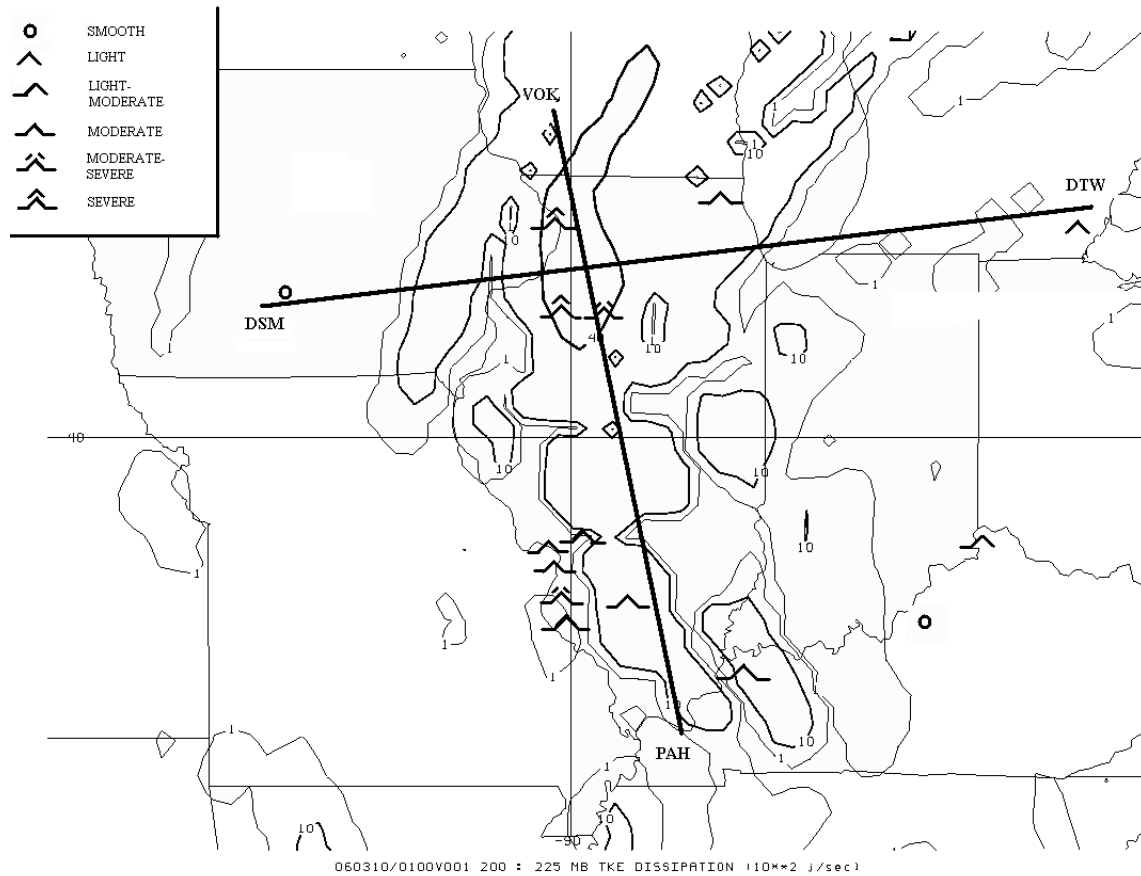


Figure 3. The ULTURB 200-225 hPa TKE production from the RUC2 forecast in Fig. 2 overlaid with PIREPs of turbulence occurring over the upper Mississippi and Ohio valleys between FL350 and FL410 for the time period from 0000 UTC to 0200 UTC, 10 March 2006. Lines indicate cross-sections used in Figure 5.

Cross-sections during this CAT outbreak also reveal the efficacy of Lighthill-Ford theory in identifying likely regions for turbulence. Figure 4 shows nearly perpendicular cross-sections from Des Moines, IA (DSM) to Detroit, MI (DTW) and Volk Field, Camp Douglas, WI (VOK) to Paducah, KY (PAH). PIREPs within 100 km of the cross section are overlaid. Spatial patterns of TKE production using Lighthill-Ford theory are relatively coherent; that is, they more closely resemble the physical wave patterns found in experiments by Williams et al. (2005) than numerical noise.

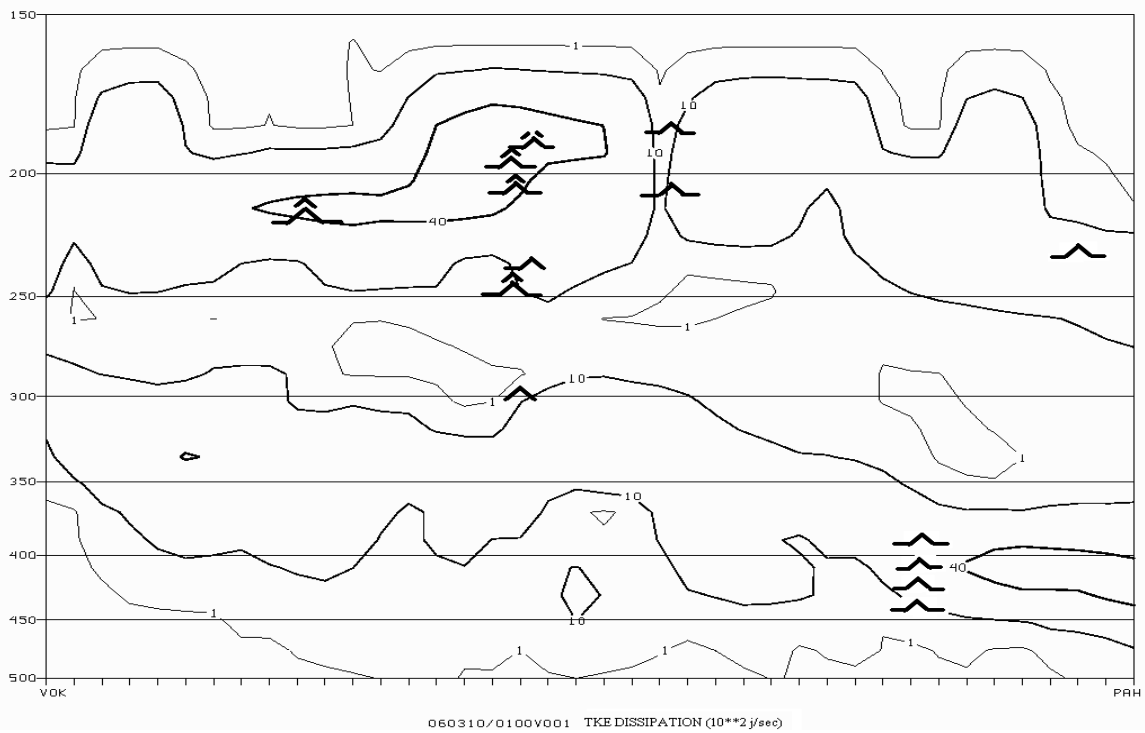
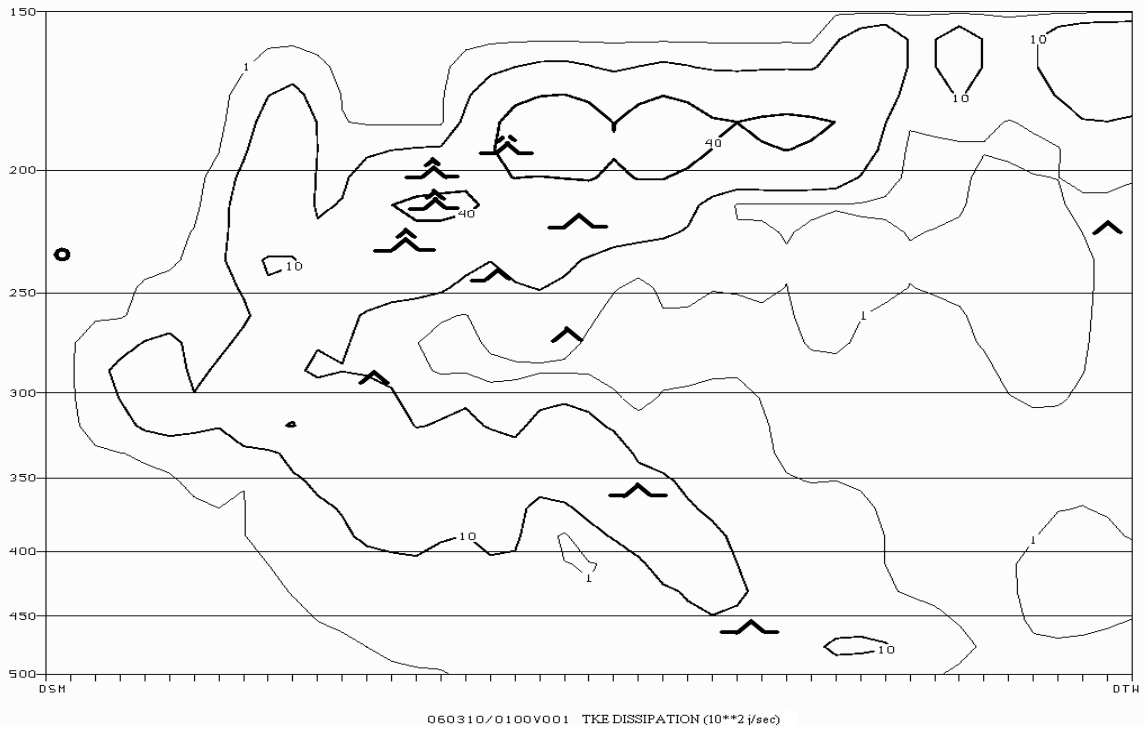


Figure 4. a) Vertical cross-section from Des Moines, IA (DSM) to Detroit, MI (DTW) of TKE dissipation using the 1-hour RUC2 forecast at 0000 UTC 10 March 2006. PIREPs within 100 km of the cross section are overlaid. b) As in a) except for a vertical cross-section from Volk Field, Camp Douglas, WI (VOK) to Paducah, KY (PAH).

This method of turbulence forecasting was used to diagnose the occurrence of turbulence during a 144-day period using the 20 km output from the 13-km RUC2 operational numerical weather prediction model. Layer TKE production rates calculated from the 1-hour forecasts from the 1500 UTC model run (valid at 1600 UTC) for each day from 3 November 2005 to 26 March 2006 are validated with text pilot reports of turbulence from 1500 UTC to 1700 UTC. There were 5446 reports at or above FL200 and 3996 below FL200. PIREPs in convection (as determined subjectively from satellite imagery) or in mountain waves (as determined from the MWAVE algorithm; McCann 2006) were not included in the database. The maximum TKE production rate in the layer with the FL within 50 km of the pilot report of CAT was matched with the subjective pilot report of the intensity of the turbulence.

One way to assess an algorithm's skill is to create a set of 2×2 contingency tables by varying the threshold chosen to make a yes-or-no forecast decision and then comparing those with the yes-or-no observed conditions (Mason 1982). For each threshold the members of the table are the number of correct yes forecasts (YY), the number of correct no forecasts (NN), the number of incorrect yes forecasts (YN), and the number of missed forecasts (NY). The Heidke Skill Score (HSS; Doswell et al. 1990) is one of many skill summary measures for 2×2 contingency tables. It gives credit for the correct forecasts (YY and NN) and deducts for the incorrect forecasts (YN and NY). The score may vary between -1 and 1, with zero meaning no skill. The HSS's strength over other summary measures is its ability to account for rare events. Because PIREPs are sparse and not random (they tend to report positive turbulence), the YN and NY categories may be uncertain. Therefore the absolute value of the HSS is not likely accurate, but it may be compared within a HSS set to assess which threshold creates the highest skill.

Figures 5 and 6 show the HSS for ULTURB at or above FL200 and below FL200, respectively, during November 2005-March 2006. They reveal a positive forecast skill for all CAT intensities at all flight levels. Especially noteworthy is that the highest score for the differentiation between no turbulence and positive turbulence is for a zero threshold. In other words, when there is positive TKE dissipation forecast, aircraft will likely feel some turbulence. At moderate and severe intensities the HSS peaks with higher TKE dissipation; this indicates that the higher the forecast TKE rate, the stronger the expected turbulence. The skill of ULTURB in the lower atmosphere is better for LIGHT and MODERATE turbulence but less than for SEVERE turbulence.

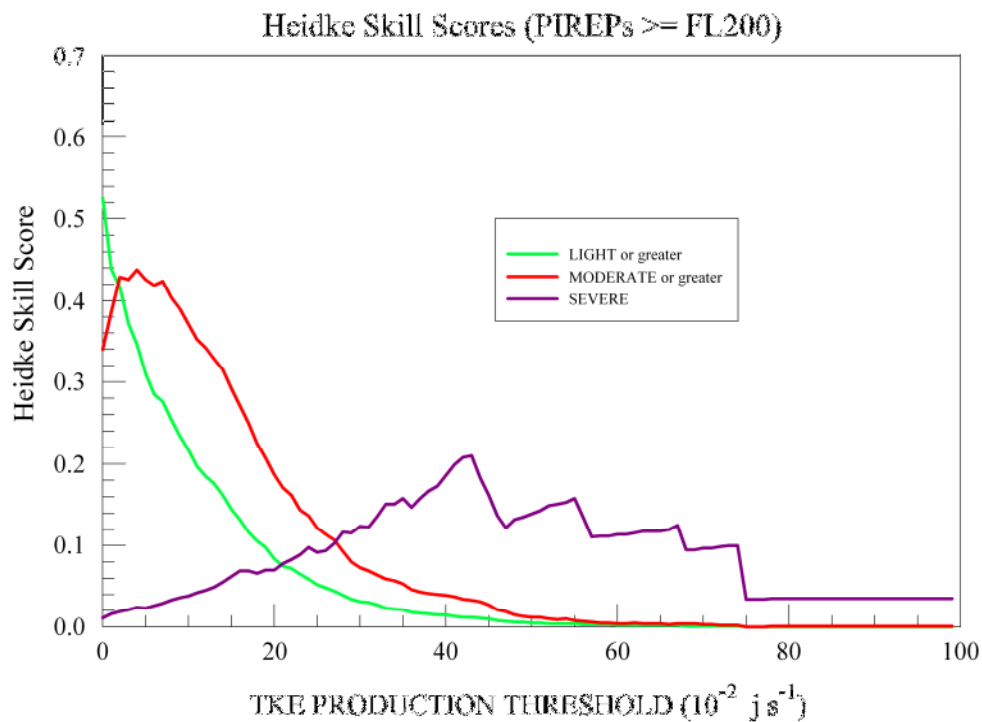


Figure 5. Heidke Skill Score (HSS) for various intensities of clear-air turbulence using ULTURB for the period 3 November 2005 to 26 March 2006. Layer TKE production rates were calculated from the 1-hour RUC2 forecasts from the 1500 UTC model run (valid at 1600 UTC) for each day, and validated with 5546 text pilot reports of turbulence from 1500 UTC to 1700 UTC at or above FL200.

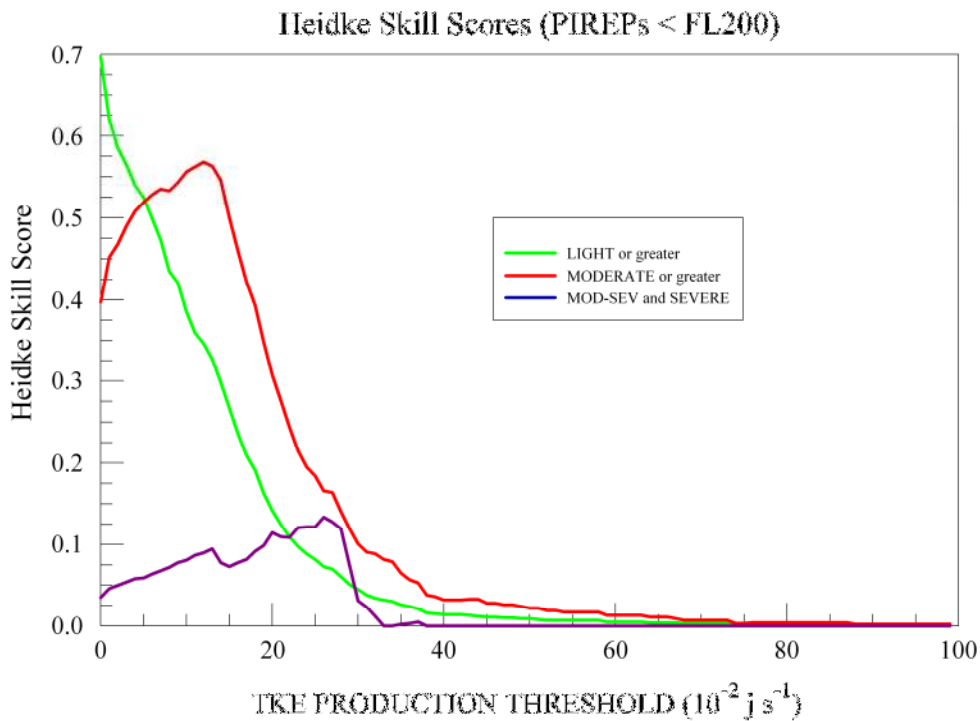


Figure 6. Same as Figure 5 except for validation of 3996 text pilot reports below FL200.

References

Bacmeister, J.T., P.A. Newman, B.L. Gary, and K.R. Chan, 1994: An algorithm for forecasting mountain wave-related turbulence in the stratosphere. *Wea. Forecasting*, **9**, 241-253.

Cornman, L. B., C. S. Morse, and G. Cuning, 1995: Real-time estimation of turbulence severity from in-situ aircraft measurements. *J. Aircraft*, **32(1)**, 171-177.

Doswell III, C. A., R. Davies-Jones, and D. Keller, 1990: On summary measures of skill in rare event forecasting based on contingency tables. *Wea. Forecasting*, **5**, 576-585.

Ford, R., 1994: Gravity wave radiation from vortex trains in rotating shallow water. *J. Fluid Mech.*, **281**, 81-118.

Knox, J.A., G.P. Ellrod, and P.D. Williams, 2006: Improved clear air turbulence diagnostics based on adjustment dynamics. *Proc. 12th Conf. on Aviation, Range, and Aerospace Meteorology*, Atlanta, GA.

Knox, J.A., D.W. McCann, and P.D. Williams, 2007: Application of the Lighthill-Ford theory of spontaneous imbalance to clear-air turbulence forecasting. Submitted to *J. Atmos. Sci.*

Lighthill, M.J., 1952: On sound generated aerodynamically, I. General theory. *Proc. Roy. Soc. London*, **211A**, 564-587.

Lilly, D.K., 1978: A severe downslope windstorm and aircraft turbulence event induced by a mountain wave. *J. Atmos. Sci.*, **35**, 59-77.

MacFarlane, N.A., 1987: The effect of orographically excited gravity wave drag on the general circulation of the lower stratosphere and troposphere. *J. Atmos. Sci.*, **44**, 1775-1800.

Mason, L., 1982: A model for assessment of weather forecasts. *Australian Meteorological Magazine*, **30**, 291-303.

McCann, D.W., 2001: Gravity waves, unbalanced flow, and aircraft clear air turbulence. *Natl. Wea. Digest*, **25(1,2)**, 3-14.

_____, 2006: Diagnosing and forecasting aircraft turbulence with steepening mountain waves. *Natl. Wea. Digest*, **30**, 77-92.

Sharman, R., C. Tebaldi, G. Weiner, and J. Wolff, 2006: An integrated approach to mid- and upper-level turbulence forecasting. *Wea. Forecasting*, **21**, 268-287.

Williams, P.D., T.W.N. Haine, and P.L. Read, 2005: On the generation of short-scale unbalanced modes in rotating two-layer flows with vertical shear. *J. Fluid Mech.*, **528**, 1-22.